Journal of Chemistry and Technologies, 2024, *32*(1), 17-29

Journal of Chemistry and Technologies

pISSN 2663-2934 (Print), ISSN 2663-2942 (Online).

journal homepage: http://chemistry.dnu.dp.ua
editorial e-mail: chem.dnu@gmail.com

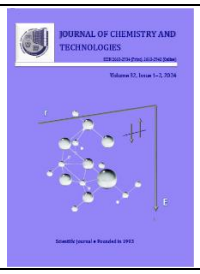

UDC 661.097.3

STRUCTURE, OPTICAL PROPERTIES AND PHOTOCATALYTIC ACTIVITY OF UNDOPED, Y_2O_3-DOPED ZnO NANOCOMPOSITES

Olga V. Chudinovych[1,2*], Liliia A. Myroniuk[1], Denys V. Myroniuk[1], Olena I. Olifan[1], Ihor M. Danylenko[3]

[1]*I. M. Frantsevich Institute for Problems in Materials Science, NAS of Ukraine, 3, Omeliana Pritsaka St., 03142, Kyiv, Ukraine*
[2]*National Technical University of Ukraine «Igor Sikorsky Kyiv Polytechnic Institute», 37, Beresteiskyi Ave., 03056, Kyiv, Ukraine*
[3] *V. Lashkaryov Institute of Semiconductor Physics of the NAS of Ukraine, 41 Nauky Av., Kyiv, 03039, Ukraine*

Received 19 August 2023; accepted 15 October 2023; available online 25 April 2024

Abstract

Y-doped ZnO nanocomposites with different content of Y_2O_3 (1–5 %) were obtained by the Pechini method from their nitrate solutions. The solutions of Zn^{2+} and Y^{3+} nitrates were preliminary obtained by dissolving of zinc and yttrium oxides with a content of the main component of 99.99% in nitric acid. The influence of yttrium doping the on the microstructure, morphology, optical properties and photocatalytic activity of the ZnO nanopowders were examined. The properties of the nanopowders were studied by using X-ray phase analysis, scanning electron microscopy (SEM), energy dispersive X-ray spectroscopy. The samples were subjected to X-ray powder diffraction using a DRON-3 diffractometer (Cu-Kα radiation) at room temperature. X-ray phase analysis confirms the formation of single phase of Y_2O_3-doped ZnO powders on diffractograms. According to SEM results, the powders characterized a conglomerate structure. The undoped ZnO has an average particle size of 43 nm, while the average particle size of Y^{3+}-doped ZnO ranges from 63 to 79 nm. It was established that the morphology of powder particles primarily depends on the content of Y^{3+} in the material. Raman scattering measurements indicate that ZnO samples doped with Y_2O_3 have an intense and clearly expressed A_1^{TO} mode, which may be related to the deformation of the powder granules. In the photoluminescence spectra of ZnO powders, with increasing Y_2O_3 concentration, bands at 400 nm are observed due to the appearance of impurities that cause of interstitial zinc and zinc vacancy defects and their broadening with a shift to the long-wave region. Photocatalytic properties of ZnO powders doped with yttrium oxide were investigated using Methyl Orange as a model dye under Osram Ultra-Vitalux lamp (300 W) irradiation. A present result indicates that the obtained powders are potential candidate for the practical application in photocatalysis.

Keywords: ZnO-Y_2O_3 nanopowders, zinc oxide, yttrium oxide, photocatalysis, degradation.

СТРУКТУРА, ОПТИЧНІ ВЛАСТИВОСТІ ТА ФОТОКАТАЛІТИЧНА АКТИВНІСТЬ НАНОКОМПОЗИТІВ ZnO, ЛЕГОВАНИХ Y_2O_3

Ольга В. Чудінович[1,2], Лілія А. Миронюк[1], Денис В. Миронюк[1], Олена І. Оліфан[1], Ігор М. Даниленко[3]

[1]*Інститут проблем матеріалознавства ім. І.М. Францевича НАН України, вул. О. Пріцака, 3, Київ, Україна, 03142*
[2]*Національний технічний університет України "Київський політехнічний інститут імені Ігоря Сікорського", просп. Перемоги, 37, м. Київ, Україна, 03056*
[3]*Інститут фізики напівпровідників ім. В.Є. Лашкарьова НАН України, просп. Науки, 45, Київ, 02000*

Анотація

Нанокомпозити ZnO, леговані Y^{3+}, з різним вмістом Y_2O_3 (1–5 %), отримано методом Печіні з нітратних розчинів. Розчини нітратів Zn^{2+} та Y^{3+} попередньо отримували розчиненням оксидів цинку та ітрію з вмістом основного компонента 99.99 % у нітратній кислоті. Досліджено вплив легування оксидом Ітрію (III) на мікроструктуру, морфологію, оптичні властивості та фотокаталітичну активність нанопорошків ZnO. Властивості нанопорошків досліджували методами рентгенофазового аналізу, скануючої електронної мікроскопії (РЕМ), енергодисперсійної рентгенівської спектроскопії. На дифрактограмах отриманих порошків ZnO, легованих Y_2O_3, присутня в основному одна фаза. За результатами СЕМ порошки мали конгломератну структуру. Нелегований ZnO має середній розмір частинок 43 нм, тоді як середній розмір частинок ZnO, легований Y^{3+}, коливається від 63 до 79 нм. Встановлено, що морфологія частинок порошку в першу чергу залежить від вмісту в матеріалі Y^{3+}. Вимірювання комбінаційного розсіяння показує, що зразки ZnO, леговані Y_2O_3, мають інтенсивну та чітко виражену моду A_1^{TO}, яка може бути пов'язана з деформацією частинок порошку. У спектрах фотолюмінесценції порошків ZnO зі збільшенням концентрації Y_2O_3 спостерігаються смуги за 400 нм, зумовлені появою домішок, які викликають дефекти міжвузлового цинку та цинкових вакансій та їх розширення зі зсувом у довгохвильову область. Фотокаталітичні властивості нанопорошків ZnO, легованих оксидом Ітрію (III), досліджували з використанням метилового оранжевого як модельного барвника з опроміненням лампою Osram Ultra-Vitalux (300 Вт). Результати досліджень вказують на те, що отримані порошки є потенційними кандидатами для практичного застосування у фотокаталізі.

Ключові слова: нанопорошки ZnO-Y_2O_3, оксид цинку, оксид ітрію, фотокаталіз, деградація.

**Corresponding author: e-mail: chudinovych_olia@ukr.net*

Journal of Chemistry and Technologies, 2024, *32*(1), 17-29

Introduction

In recent years, the development of new advance photocatalytic materials has become the objects of intensive scientific research. Photocatalytic materials based on metal oxides are distinguished among other materials by their high chemical resistance, mechanical strength and non-toxicity. Therefore, the production of new oxide photocatalytic materials is an urgent problem.

Photocatalytic decomposition of organic substances occurs when they are in close contact with a photoactive material. Therefore, the contact area is very important for efficient photocatalysis. This determines the significant influence of the morphology of materials on their photocatalytic activity. Thus, it was established that the photocatalytic activity strongly increases with the dispersion of materials. In many works, the objects of research of photocatalytic properties were oxide powders [1–18].

It is well known that ZnO-based materials exhibit high photocatalytic properties. They are promising candidates for practical application. It was established that the photocatalytic and bactericidal properties of ZnO-based materials depend on their morphology and can be enhanced by the addition of some materials (CdS, CeO_2, TiO_2, SnO_2, In_2O_3, Ag_2) [19]. Rare earth elements also are used as dopants for synthesis of photocatalytic materials [1–21]. The addition of rare earth elements increased the photoactive properties of oxide materials based on TiO_2 and ZnO [19]. It was established [19–20] that small additions of Y_2O_3 dramatically increase the bactericidal properties of transparent coatings based on ZnO. The combination of ZnO with Y^{3+} ions in the form of ZnO-Y_2O_3 nanostructures involves increasing its photocatalytic activity, creating transparent coatings for displays, improving UV radiation in photoluminescence (PL), etc. The element yttrium (Y) has one filled 4d orbital, which creates certain electron configurations. Its oxides have numerous advantages, including different types of crystallinity, as well as good electronic conductivity and thermal stability [14; 22]. In the study [15], ZnO nanopowders doped with different concentrations of Y^{3+} ions were obtained using a simple combustion method. In this work, was shown that the inclusion of Y^{3+} ions improves the photocatalytic characteristics of ZnO. The percentage of photocatalytic degradation of Phenol (Ph), Methylene Blue (MB), and Rhodamine B (RhB) by ZnO nanoparticles doped with Y_2O_3 reaches 91 %, 94 %, and 97 %, respectively within 90 min under the influence of visible irradiation. The highest rate of photocatalytic decomposition of Phenol, MB, and RhB solutions (98 %) was obtained after 40 minutes using ZnO doped with 1 % Y_2O_3. In [16], dense nanocrystalline ZnO containing 1 and 5 mol.% was obtained by microwave irradiation. % of yttrium oxide and its UV catalytic activity was investigated. The photodegradation reaction kinetics of MB dyes showed first-order reaction kinetics for ZnO samples doped with 1 mol. % Y_2O_3. When the doping of Y_2O_3 exceeded 5 mol. %, the catalytic reaction was described as a second-order reaction. The reason was the segregation of Y_2O_3 [16].

According to these research results, the properties of the photocatalytic materials are sensitive to the conditions of their preparation. Hence, metal impurity can increase or decrease the photocatalytic activity of ZnO depending on the preparation conditions and doping concentrations [23]. Based on the above, the effect of Y^{3+} doping on the structural, optical and photocatalytic properties of ZnO nanopowders obtained by Pechini method was investigated. In this work, the photocatalytic properties of Y_2O_3-doped ZnO nanopowders were studied by the decomposition of Methyl Orange dye at Osram Ultra-Vitalux lamp irradiation. The detailed study of photocatalytic properties of ZnO nanopowders doped with rare earth oxides can also be of both scientific interest and practical importance.

Experimental

Y_2O_3-doped ZnO nanocomposites were obtained by the Pechini method. The essence of the method is to achieve a high degree of cations mixing in the solution, the controlled transition of the solution into a polymer gel, the removal of the polymer matrix with the formation of an oxide precursor, and the preservation of a high degree of homogeneity. Solutions of Zn^{2+} and Y^{3+} nitrates, which were obtained by dissolving zinc and yttrium oxides with a content of the main component of 99.99 % in nitric acid, were used as starting materials. Before preparing the initial solutions, yttrium oxide was pre-dried in a muffle at 300 °C for 2 hours. A mixture with different Y^{3+} content was prepared from nitrate solutions. The mix of nitrate and citric acid solutions was stirred for 1 hour at 80 °C. The obtained precursor was dried at 150 °C for 24 hours and then subjected to heat treatment at 800 °C.

Journal of Chemistry and Technologies, 2024, *32*(1), 17-29

The samples were subjected to X-ray powder diffraction using a DRON-3 diffractometer at room temperature (Cu-Kα radiation). The scan angle was 0.05–0.1 ° in the range 2θ = 15–90 °. The lattice parameters were calculated with the least-square method employing the LATTIC software, with an error of less than 0.0002 nm for the cubic phase. The phase composition was determined of the Joint Committee on Powder Diffraction Standards (JCPDS International Center for Diffraction Data, 1999).

The volume of the unit cell was determined using the calculation data of the cell parameters obtained by the X-ray method [24]:

- cubic symmetry: $V_{ek} = a^3$
- monoclinic symmetry: $V_{ek} = a \cdot b \cdot c \cdot sin\beta$
- hexagonal symmetry: $V_{ek} = 0{,}866 \cdot a^2 \cdot b$
- rhombic symmetry: $V_{ek} = a \cdot b \cdot c$.

Scanning electron microscopy (SEM) was used to assess the homogeneity of the powders. Elemental analysis of the samples was performed by X-ray spectral microanalysis (XMR) using an energy dispersive spectrometer (EDS) INCA 450 (OXFORD Instruments). The atomic concentrations of the elements were determined within the relative experimental error of ~ 0.2 % for the investigated area of 500 μm x 500 μm.

The specific surface area of the samples was measured by the chromatographic method of low-temperature argon adsorption at –196 °C (one-point BET method). The essence of the method is that test samples are analyzed under identical conditions with a standard sample with a specific surface area known and stable over a long time. In this case, silica (cytochrome C-80) with a specific surface area of 80 m^2/g was used as a standard.

Raman scattering and photoluminescence (PL) spectra were recorded by Horiba Jobin Yvon T64000 spectrometer equipped with a CCD detector at room temperature. Radiation from solid-state lasers (442 and 532 nm) and the He-Cd laser (325 nm) was focused onto the sample using an Olympus BX 41 microscope and used to study Raman scattering and PL. At the same time, the diameter of the analyzed spot was 1 μm, and the spectral resolution was 1 cm^{-1}.

The photocatalytic activity of zinc oxide powders doped with yttrium oxide was studied by the decomposition of Methyl Orange (MO), which was used as a model dye. Powders of undoped zinc oxide and doped with Y_2O_3 (1–5 %) were dispersed in an aqueous solution of MO with an initial concentration of 10 mg/L. The resulting suspensions were stirred using a magnetic stirrer for 30 min in the dark until adsorption-desorption equilibrium was reached between Methyl Orange and the catalyst surface. The content of the catalyst powder in the MO solution was 2 g/L. The samples were irradiated with Osram Ultra-Vitalux lamp with a power of 300 W for 30, 60, 90, and 120 minutes, respectively (Fig. 1). After the specified time intervals, 5 ml of the suspension were filtered to remove the photocatalyst, and transmission spectra were measured on a modern two-beam UV spectrophotometer Shimadzu UV2600i. Distilled water was used as a standard. MO has two absorption peaks in distilled water at 270 nm and 465 nm, respectively. The concentration of MO dye was monitored by measuring the transmission of visible absorption at 465 nm at each stage of photodegradation. According to the Beer-Lambert law, MO concentration is linearly proportional to the transmittance value (T) at 465 nm [25]. The concentration of MO in the investigated solutions was determined by measuring of the transmission coefficient at 465 nm.

Degradation efficiency (DE) was calculated according to equation (1):

$$DE = \frac{C_0 - C}{C_0} \times 100, \qquad (1)$$

where C_0 is the initial dye concentration, C is the concentration after photoirradiation.

The reaction kinetics of the MO dye degradation was described by the pseudo-first order model (2):

$$ln\,(C/C_0) = -k \times t, \qquad (2)$$

where C_0 and C are the concentrations of MO dye in the aqueous solution at time t = 0 and certain time t respectively, and k is the pseudo-first order degradation rate constant [26]. The error of dye concentration measurement was no more than 0.1.

Journal of Chemistry and Technologies, 2024, *32*(1), 17-29

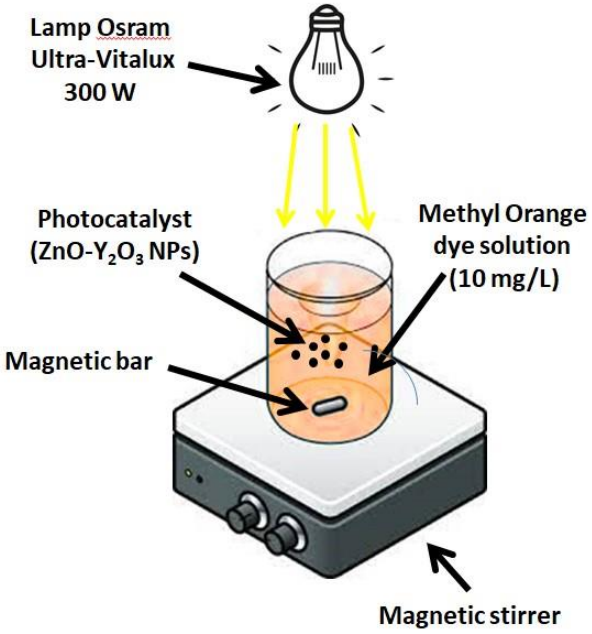

Fig. 1. Photocatalytic activity testing system

Results and Discussion

Structural properties

Fig. 2 shows XRD patterns of ZnO and Y_2O_3-doped ZnO nanocomposites in the samples with from 1 to 5 % Y_2O_3 presence of peaks corresponding to Y_2O_3. This indicates the not ideal solubility and not homogeneity of Y^{+3} ions in the ZnO lattice.

All samples have a polycrystalline structure corresponding to the hexagonal phase of wurtzite ZnO. The diffractograms are indexed by ICDD card No. 01-036-1451 (a = 0.3250 nm, c = 0.5206 nm). The main peaks belong to the planes (100), (002), (101), (102), (110), (103), (200), (112), (201), (004), and (202). The Y^{+3} amount increase in zinc oxide leads to a change, namely an increase in the lattice period (Table 1, Fig. 3). This increase can be explained by the size factor of the Y^{+3} ions radius (0.089 nm) is greater than the Zn^{+2} ions radius (0.074 nm).

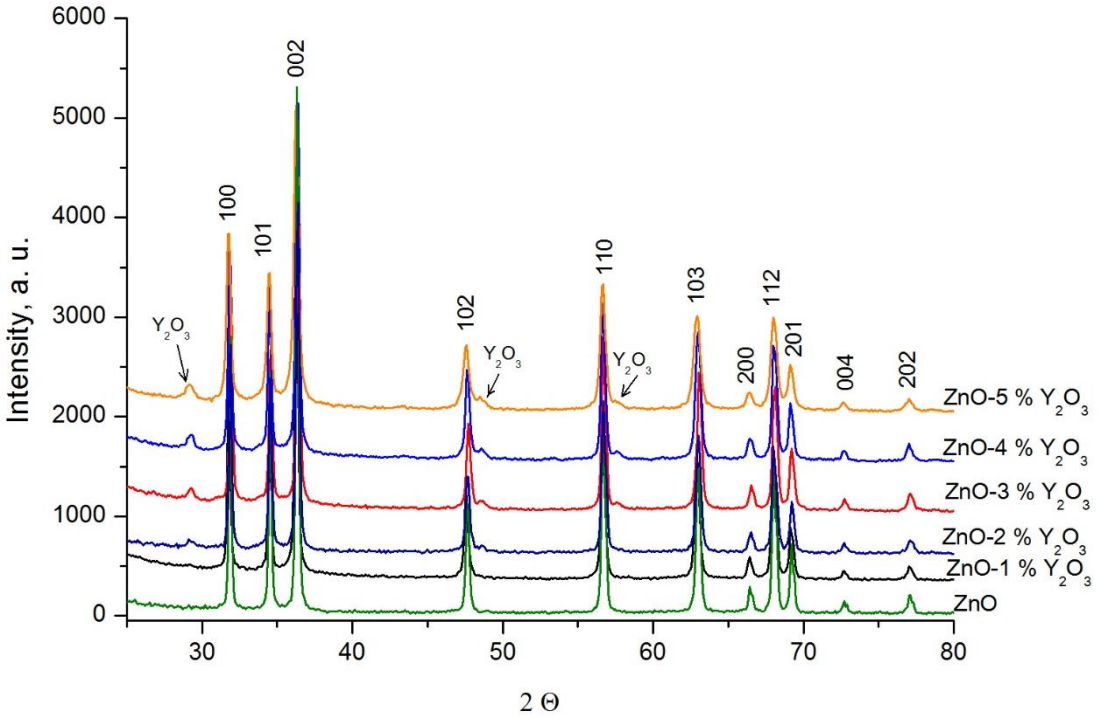

Fig. 2. XRD patterns of ZnO and Y_2O_3-doped ZnO nanocomposites

Journal of Chemistry and Technologies, 2024, *32*(1), 17-29

Table 1

Structural properties of Y_2O_3-doped ZnO nanocomposites

Sample	Lattice parameters of the phases, nm		*c/a*	Cell volume V, nm³
	a	*c*		
ZnO	0.3248	0.5200	1.601	0.0475
ZnO-1 % Y_2O_3	0.3248	0.5201	1.601	0.0475
ZnO-2 % Y_2O_3	0.3246	0.5202	1.602	0.0475
ZnO-3 % Y_2O_3	0.3244	0.5204	1.604	0.0474
ZnO-4 % Y_2O_3	0.3247	0.5204	1.603	0.0475
ZnO-5 % Y_2O_3	0.3250	0.5206	1.602	0.0476

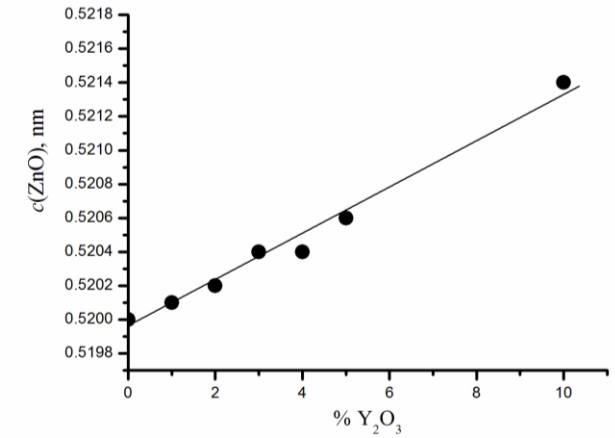

Fig. 3. Dependence of the unit cell parameter c of zinc oxide on the Y_2O_3 content

Structurally, ZnO has three types of crystal planes, two non-polar (2110) and (0110) planes and a polar (0001) basal plane with C6V symmetry. The (0001) plane has a higher surface energy, so crystal growth in the direction of the c-axis is faster, which leads to the formation of nanorod-shaped crystals, as shown in Fig. 4a. A change from a nanorod to a nanoplate form is observed after doping ZnO with trivalent ions of rare earth elements (Fig. 4b) [27].

The presence of trivalent ions instead of Zn^{2+} ions in the ZnO crystal is likely to increase the adsorption of ligands on these basal surfaces, which in turn will lead to a decrease in the growth rate of ZnO nanocrystallites along the c-axis direction. This means that crystal growth along the (0001) direction is significantly suppressed under this condition, while nanocrystallites can still grow along the (2110) direction. The scheme of disruption of the crystal structure of the ZnO lattice by doping is shown in Fig. 4c, which shows the crystal growth oriented along the lateral directions. Therefore, the sharp morphological changes observed for ZnO samples doped with trivalent ions can be considered evidence of the inclusion of these elements in the ZnO lattice.

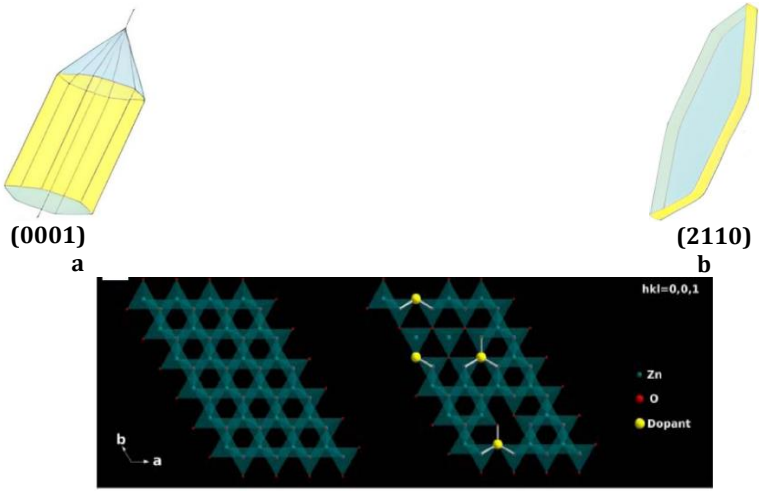

c

Fig. 4. Schematic crystal growth of pure (a) and doped (b) ZnO nanostructures. Scheme of crystal growth in lateral directions after doping (c) [27]

Journal of Chemistry and Technologies, 2024, *32*(1), 17-29

Adsorption-structural studies

The specific surface area of the samples was measured by the chromatographic method of low-temperature argon adsorption at -196 °C (one-point BET method). The value of the particular surface of the test sample was calculated according to the formula:

$$S_{BET} = (S \cdot F_c \cdot m_c) / (F \cdot m),$$

where S_{BET} and S are the specific surfaces of the sample and standard, respectively, m^2/g; F and F_c are the areas of the argon desorption peak of the studied sample and the standard, respectively (chromatographic data); m and m_c are the mass of the sample and the standard, respectively, g.

Table 2

Specific surface area of Y_2O_3-doped ZnO nanocomposites

Composition	S_{BET}, m^2/g
ZnO	3.8
ZnO-1 % Y_2O_3	6.0
ZnO-2 % Y_2O_3	5.1
ZnO-3 % Y_2O_3	6.8
ZnO-4 % Y_2O_3	5.7
ZnO-5 % Y_2O_3	9.5

The morphology and chemical composition study

According to SEM, the synthesized powders have a conglomerate structure. Particles whose size does not exceed 100 nm are observed in the conglomerate themselves (Fig. 5).

The morphology of powder particles primarily depends on the content of Y^{3+} in the material. The undoped zinc oxide characterized particles with regular shape from 20 to 50 nm, and average size - 43 nm. The small amounts of single particles with diameter of 5 nm are also observed (Table 3). The introduction of Y^{3+} affects changes in particle morphology and size. The particles began to acquire a lamellar shape, and their average planar dimensions increased to 79 nm.

Table 3

Size of Y_2O_3-doped ZnO nanocomposites

Composition	Size, nm
ZnO	43
ZnO-1 % Y_2O_3	74
ZnO-2 % Y_2O_3	79
ZnO-3 % Y_2O_3	64
ZnO-4 % Y_2O_3	68
ZnO-5 % Y_2O_3	63

Raman scattering

Raman scattering measurements were carried out to investigate the influence of Y^{3+} doping on the structural and vibrational properties of ZnO powders.

According to group theory, ZnO with wurtzite structure belongs to space group C^4_{6v} with two formula units per unit cell. The unit cell of ZnO consists of four atoms, each of which occupies the C_{3v} position, leading to 12 phonon branches (nine optical and three acoustic). The irreducible expression of optical phonons is given as $\Gamma_{opt}=A_1+2B_1+E_1+2E_2$. Modes A_1 and E_1 are polar and can be divided into transverse-optical (TO) and longitudinal-optical (LO) phonons, while modes B_1 are Raman inactive [28]. The oscillation of A_1 phonons is polarized parallel to the *c* axis; phonon E_1 is polarized perpendicular to the *c* axis. Each mode corresponds to a band in the Raman spectrum. The intensity of these bands depends on the cross section of the scattering of these modes. The nonpolar modes E_2 are Raman active and have two wavenumbers, namely low – E_2^{low} and high – E_2^{high}, associated with the motion of the the zinc (Zn) and oxygen (O) sublattice, respectively.

Fig. 6 shows Raman light scattering spectra for zinc oxide nanopowders doped with yttrium oxide. In all ZnO-Y_2O_3 powders, typical E_2^{high} and E_2^{low} Raman scattering modes are clear detected, A_1^{TO}, A_1^{LO} modes and combinations of E_2^{high}-E_2^{low} and $E_1^{TO}+E_2^{low}$ are observed.

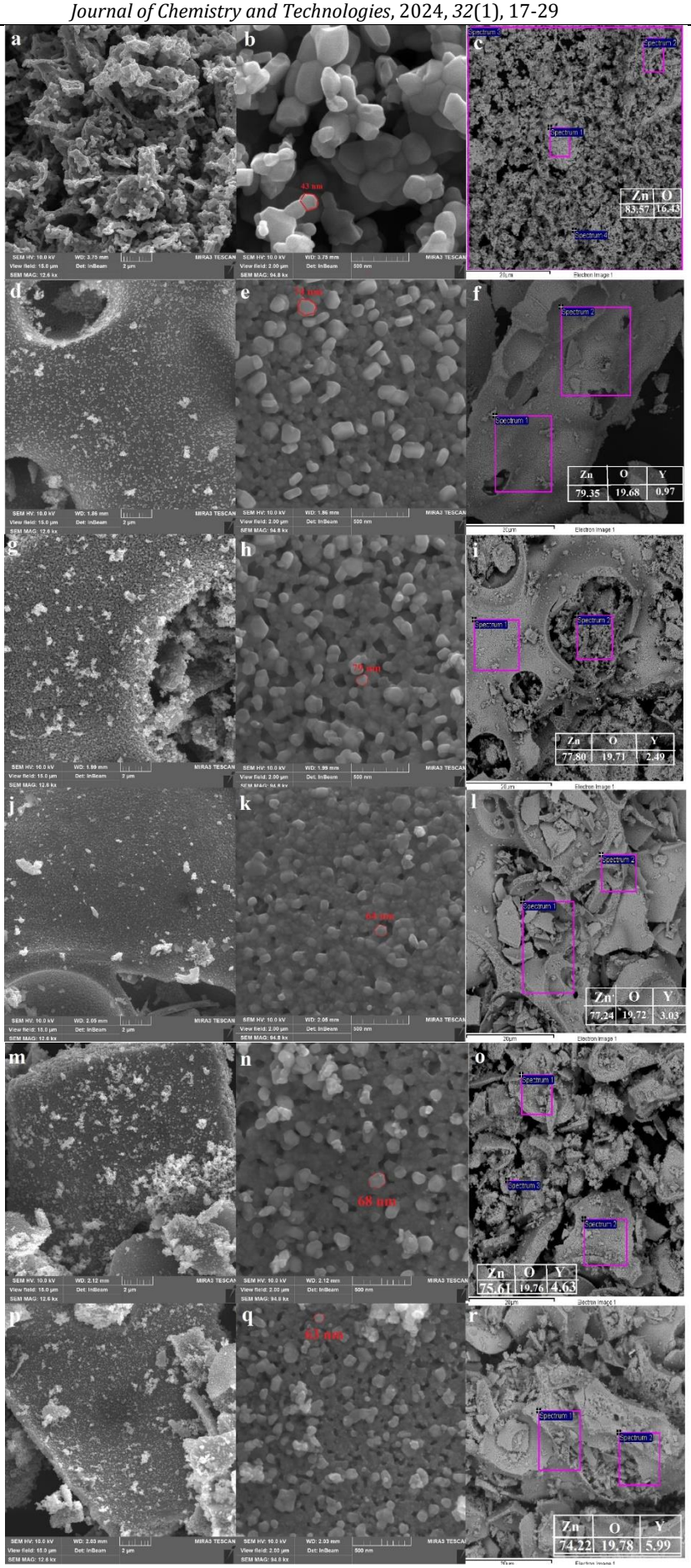

Fig. 5. Powders of pure zinc oxide (a, b, c) and doped with 1 % Y^{3+} (d, e, f), 2 % Y^{3+} (g, h, i), 3 % Y^{3+} (j, k, l), 4 % Y^{3+} (m, n, o), 5 % Y^{3+} (p, q, r).

Journal of Chemistry and Technologies, 2024, *32*(1), 17-29

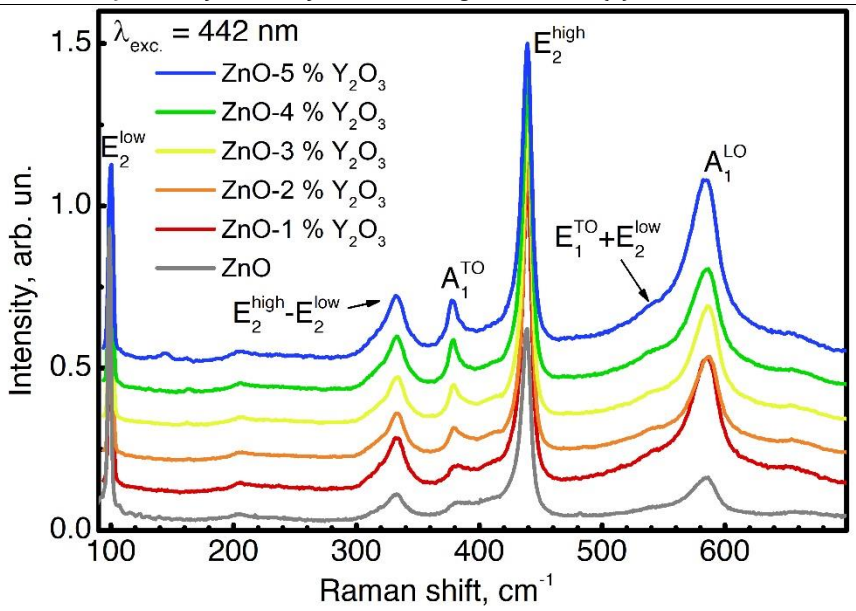

Fig. 6. Raman scattering spectra of ZnO powders doped with yttrium oxide (1-5 %).

A noticeable increase in the intensity of the A_1^{LO} mode is observed with increasing concentrations of yttrium oxide in the powders. For high quality ZnO films the intensity of A_1^{LO} mode is weak due to a destructive interference between the deformation and Fröhlich contributions to the LO scattering cross-section. In our case, the high intensity of A_1^{LO} mode is caused by a ZnO lattice disorder [29]. The samples with yttrium oxide also have a more intense and more clearly expressed A_1^{TO} mode, which may be related to the deformation of the powder granules.

In samples with 2 and 5 % by weight of yttrium oxide bands of intracentric luminescence are detected, which are observed only upon excitation by a 532 nm solid-state laser, which with a high probability can be associated with the formation of Y_2O_3 clusters and an increase in the yttrium content at the grain boundaries (Fig.7).

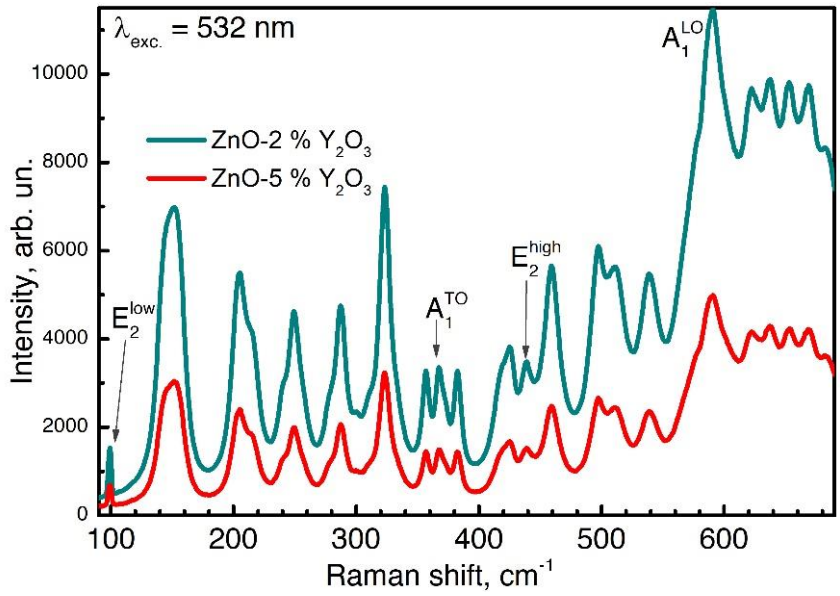

Fig. 7. Raman scattering spectra of ZnO powders doped with Y_2O_3 (2 % and 5 %)

Photoluminescence (PL) studies

In the PL spectra of ZnO powders a near bandgap edge emission around 389 nm and a deep-level emission associated with transitions from defects at 560 nm were observed [30]. The relatively narrow maximum in the UV region around 385 nm in the samples corresponds to the emission during the recombination of free excitons [31]. With increasing Y_2O_3 concentration, bands at 400 nm are observed due to the appearance of impurities that cause of

Journal of Chemistry and Technologies, 2024, *32*(1), 17-29

interstitial zinc and zinc vacancy defects and their broadening with a shift to the long-wave region.

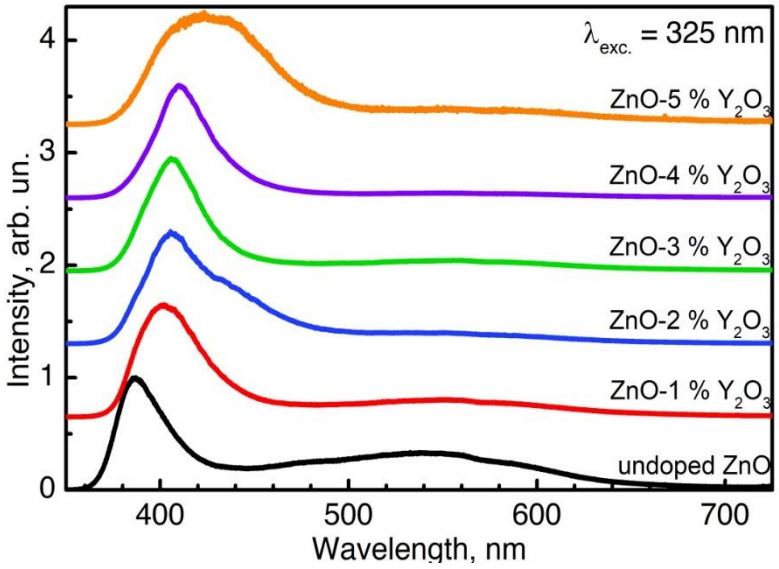

Fig. 8. Photoluminescence spectra of ZnO and Y-doped ZnO (1-5%) nanopowders

Study of the photocatalytic activity of ZnO and Y_2O_3-doped ZnO nanopowders

Photocatalytic activities of undoped and doped with 1–5 % yttrium oxide ZnO nanopowders (NPs) were studied by the decomposition of aqueous Methyl Orange (MO) dye solution. Methyl orange belongs to the organic azo dyes groups, which are widely used in printing, textile, and other industries. Its entry into the environment has a toxic effect on living organisms and, in particular, a carcinogenic effect on humans [28]. In order to studying the photocatalytic activity of Y_2O_3-doped ZnO NPs, the powder catalyst was dispersed in a aqueous solution of MO (10 mg/L) and were exposed under Osram Ultra-Vitalux lamp irradiation with power of 300 W during 30, 60, 90 and 120 min.

In fig. 9 presents the photodegradation kinetics of MO dye by ZnO and Y_2O_3-doped ZnO NPs. The obtained results indicated that the Y^{3+}-doped ZnO NPs has a lower photocatalytic activity compared to undoped ZnO NPs. The photocatalytic efficiency of pure zinc oxide powders consist 96.6 % after 120 min of irradiation. At the same time, the photocatalytic activity of ZnO NPs powders doped with Y_2O_3 (1 and 2 wt. %) is 79.2–79.9 %. For ZnO NPs with a higher concentration of yttrium oxide impurity (3–5 % wt. %), this value decreased to 63–66 % (Fig. 10). The reason of the reducing in the photocatalytic activity of Y-doped ZnO nanopowders compared to pure ZnO can be due to increasing of ZnO particles size after yttrium doping. A further decrease in the photocatalytic activity of doped ZnO nanopowders can be associated with the introduction of an excess amount of Y^{3+} (3–5 wt. %), which leads to the formation of the second phase of yttrium oxide (Fig. 2). From the obtained results, it can be concluded that the optimal dopant concentration of Y^{3+} is not more 1–2 %wt. Therefore, the selection of the obtaining conditions (method and concentration of impurity) of doped zinc oxide powders plays an important role in creating a material with the necessary photocatalytic properties. In this case, the reduction of photocatalytic properties can also be of practical importance. The use of materials based on zinc oxide with reduced photocatalytic activity is promising for slowing down the decomposition of pigments under the influence of UV radiation.

The degradation rate constant k were determined from the slope of the curves and equation $ln(C/C_0) = -kt$. Fig. 11 presents the dependence of degradation rate constant k *vs* yttrium concentration The reaction kinetics of the MO dye destruction could be described by the pseudo-first order model for low dye concentrations, where C_0 and C are the concentrations of MO at time $t=0$ and certain time t, respectively, k is the pseudo-first order rate constant [32].

Journal of Chemistry and Technologies, 2024, *32*(1), 17-29

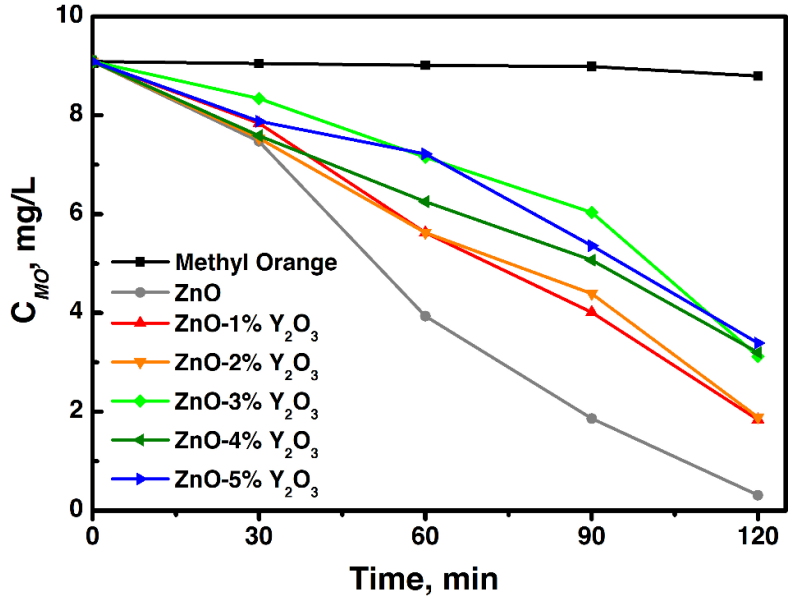

Fig. 9. Kinetics of MO dye photodegradation by undoped and Y_2O_3-doped ZnO nanocomposites under Osram Ultra-Vitalux 300 W lamp irradiation.

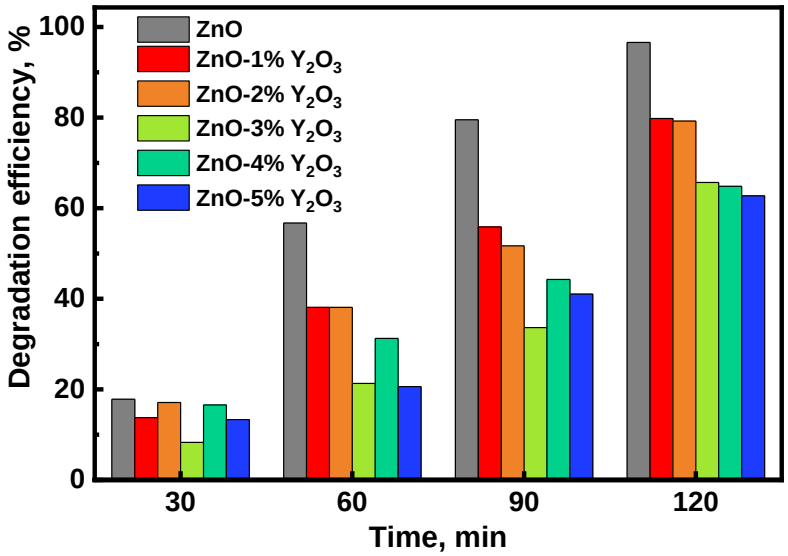

Fig. 10. Degradation efficiency (%) of Methyl Orange by ZnO and ZnO-Y_2O_3 (1–5 %)

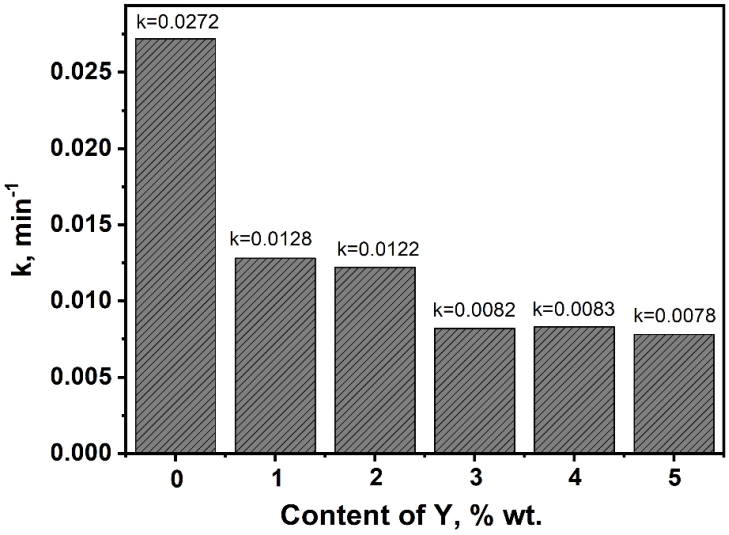

Fig. 11. Degradation rate constant (*k*) *versus* Y^{3+} content in ZnO nanopowders.

Journal of Chemistry and Technologies, 2024, *32*(1), 17-29

The obtained straight lines showing that the reactions are of pseudo-first order. The calculated values of the degradation rate constant *k* for ZnO samples doped with yttrium oxide consists 0.0078–0.0128 min^{-1}, for undoped ZnO – 0.0272 min^{-1}. As we can see from XRD and SEM results, the decrease in degradation rate constant of nanopowders doped with yttrium oxide is due to an increase in the size of the powder nanoparticles. As a result, the surface area of the photocatalyst decreases. Photocatalytic materials with a developed surface area characterized by a large number of active sites that are catalytically active and promote the separation efficiency of the electron-hole pairs in the photocatalytic reactions [33]. Photocatalytic reactions proceed with the help of OH• and O^{2-} radicals, formed on the surface of ZnO doped with Y^{3+}. During photocatalysis, the Y^{3+} ion absorbs an electron and inhibits electron-hole recombination, contributing to the following redox reactions (3–9):

$$Y^{3+} + h\nu \rightarrow \bar{e}\ (Y^{3+}) + h^{+}(\ Y^{3+}) \quad (3)$$

$$Zn^{2+} + h\nu \rightarrow \bar{e}\ (Zn^{2+}) + h^{+}(Zn^{2+}) \quad (4)$$

$$Y^{3+} + OH^{-} \rightarrow Y^{2+} + OH^{\cdot} \quad (5)$$

$$OH^{\cdot} + M\ O \rightarrow Products\ of\ photodegradation \quad (6)$$

$$Y^{3+} + \bar{e} \rightarrow Y^{2+} \quad (7)$$

$$Y^{2+} + O_2 \rightarrow Y^{3+} + O_2^{-} \quad (8)$$

$$O_2^{-} + M\ O \rightarrow Products\ of\ photodegradation \quad (9)$$

Superoxide ions O^{2-} cause the decomposition reaction as mentioned above. The presence of Y^{3+} ions contributes to the photon absorption of MO, as these ions capture electrons and inhibit electron-hole recombination. In some cases, the reducing of the photocatalytic properties of ZnO has the practical use as UV protection applications, where ZnO used as a safe and durable shielding agent against UV irradiation, because UV causes cells damage, deterioration of paints and plastics as well as color fading of paints and fabrics [34].

Conclusions

It is shown that Y-doped ZnO nanocomposites (1–5 %) characterized by a wurtzite structure of crystal lattice. An increase in the amount of Y^{3+} in zinc oxide leads to an increase in the lattice period. According to scanning electron microscopy, the synthesized powders have a conglomerate structure. It was established that the morphology of powder particles primarily depends on the content of Y^{3+} in the material. The particles began to acquire a lamellar shape and their average planar dimensions increased to 79 nm. An increase in the amount of Y^{3+} in zinc oxide leads to an increase in the specific surface area (from 3.8 to 9.5 m^2/g).

In our research, it was demonstrated that ZnO doping with Y_2O_3 (1-5 %) leads to reducing in the photocatalytic activity of obtained nano/composites/ (powders) due to decrease in the surface area of Y-doped nanopowders. As confirmed by the results of Raman scattering and photoluminescence, the decrease in photocatalytic activity of Y-doped ZnO nanopowders can be associated with the appearance of a large number of defects in the ZnO structure, caused by Y^{3+} ions excessive doping.

Acknowledge

This work supported by the research project of the NAS of Ukraine “Creation of promising materials based on ZnO doped REE for use in catalysis”

References

[1] Gupta, J., Hassan, P., Barick, K. (2021). Structural, photoluminescence, and photocatalytic properties of Mn and Eu co-doped ZnO nanoparticles. *Mater. Today: Proc.*, 42(2), 926–931. https://doi.org/10.1016/j.matpr.2020.11.837

[2] Kumawat A., Chattopadhyay S., Verma R. K., Misra K.P. (2022). Eu doped ZnO nanoparticles with strong potential of thermal sensing and bioimaging. *Mater. Lett., 308*(8), 131–221. https://doi.org/10.1016/j.matlet.2021.131221

[3] Gnanaprakasam A., Sivakumar V., Thirumarimurugan M. (2018). Investigation of Photocatalytic Activity of Nd-Doped ZnO Nanoparticles Using Brilliant Green Dye:Synthesis and Characterization. *Iran. J. Chem. Chem. Eng*., 37, 61 71. https://doi.org/10.30492/ijcce.2018.30658

[4] Lili H., Shenmao Z., Yuequan D. (2019). Preparation of rare earth Nd-doped ZnO nano-materials and its degradation of Rhodamine B. *Inorganic Chemicals Industry, 51*(8), 88–92. https://doi.org/10.11962/1006-4990.2019-0139

[5] Upadhyay P. K., Sharma N., Sharma S., Sharma R. (2021). Photo and thermoluminescence of Eu doped ZnO nanophosphors. *J. Mater. Sci.: Mater. Electron.,* 32, 17080–17093. https://doi.org/10.1007/s10854-021-06043-w

[6] Gong X., Jiang H., Cao M., Rao Z., Zhao X. Vomiero A. (2021). Eu-doped ZnO quantum dots with solid-state

fluorescence and dual emission for high-performance luminescent solar concentrators. *Mater. Chem. Front*., 5, 4746–4755. https://doi.org/10.1039/D1QM00178G

[7] Khataee A., Karimi A., Zarei M., Joo S. (2020). Eu-doped ZnO nanoparticles: Sonochemical synthesis, characterization, and sonocatalytic application. *Ultrason. Sonochem.,* 67, 102822. https://doi.org/10.1016/j.ultsonch.2015.03.016

[8] Satpal, S.B., Athawale, A.A. (2018). Synthesis of ZnO and Nd doped ZnO polyscales for removal of rhodamine 6G dye under UV light irradiation. *Mater. Res.Express*, *5*, 085501. https://doi.org/10.1088/2053-1591/AAD26C

[9] Sin, J. C., Lam, S. M. (2018). One-dimensional ZnO nanorods doped with neodymium for enhanced resorcinol degradation under sunlight irradiationvol. *Chem. Eng. Commun.,* 205, 311–324. https://doi.org/ 10.1080/00986445.2017.1387855. 24.

[10] Samanta, A., Goswami, M. N., Mahapatra, P. K. (2019). Influence of Nd^{3+} doping in ZnO nanoparticles to enhance the optical and photocatalytic activity. *Mater. Res.Express*, 6, 065031. https://doi.org/ 10.1088/2053-1591/ab0c25

[11] Kayani, Z. N., Amir, B., Riaz, S., Naseem, S. (2020). Antibacterial, magnetic, optical and dielectric analysis of novel La_2O_3 doped ZnO thin films. *Opt. Mater.*, 109, 110–287. https://doi.org /10.1016/j.optmat.2020.110287

[12] Li, C., Hun, R., Qin, L., Ding, R., Li, X., Wu, H. (2013). Enhanced photocatalytic activity of ZnO/La_2O_3 composite modified by potassium for phenol degradation. *Mater. Lett.*, 113, 190–194. https://doi.org /10.1016/j.matlet.2013.09.050

[13] Kayani, Z. N., Benish, A., Riaz, S., Naseem, S. (2020). Antibacterial, magnetic, optical and dielectric analysis of novel La_2O_3 doped ZnO thin films. *Opt. Mater.*, 109, 110–287. https://doi.org /10.1016/j.optmat.2020.110287

[14] Hsieh, P.-T., Chuang, R.-K., Chang, C.-Q., Wang, C.-M., Chang, S.-J. (2011). Optical and structural characteristics of yttrium doped ZnO films using sol-gel technology. *J. Sol-Gel Sci. Technol.*, 58, 42–47. https://doi.org 10.1007/s10971-010-2352-0

[15] AlAbdulaal, T.H., AlShadidi, M., Hussien, Mai S. A., Vanga, G., Bouzidi, A., Rafique, S., Algarni, H., Zahran, H.Y., Abdel-wahab, M.Sh., Yahia, I.S. (2021). Structural, morphological and optical bandgap analysis of multifunction applications of Y_2O_3-ZnO nanocomposites: Varistors and visible photocatalytic degradations of waste water. *Research Square*, https://doi.org/10.21203/rs.3.rs-391412/v1

[16] Sanoop, P. K., Anas, S., Ananthakumar, S., Gunasekar, V., Saravanan, R., Ponnusami, V. (2016). Synthesis of yttrium doped nanocrystalline ZnO and its photocatalytic activity in methylene blue degradation. *Arabian J. Chem.*, 9, 1618–1626. https://doi.org/10.1016/j.arabjc.2012.04.023

[17] Divya, N. K., Pradyumnan, P. P. (2016). Solid state synthesis of erbium doped ZnO with excellent photocatalytic activity and enhanced visible light emission. *Mater. Sci. Semicond. Process.*, 41, 428–435 https://doi.org/10.1016/j.mssp.2015.10.004

[18] Zong Y., Li, Zhe, Wang, X., Ma, J., Men, Y. (2014). Synthesis and high photocatalytic activity of Eu-doped ZnO nanoparticles. *Ceram. Int.*, 40, 10375–10382. https://doi.org/10.1016/j.ceramint.2014.02.123

[19] Boltenkov, I.S., Kolobkova, E.V., Evstropiev, S.K. (2018). Synthesis and characterizationof transparent photocatalytic ZnO-Sm_2O_3 and ZnO-Er_2O_3 coatings. *J. Photochem. Photobiol. A,* 367, 458–464. https://doi.org/10.1016/j.jphotochem.2018.09.016

[20] Evstropiev, S.K., Karavaeva, A.V., Dukelskii, K.V., Evstropyev, K.S., Nikonorov, N.V., Kolobkova, E.V. (2018). Transparent ZnO-Y_2O_3 coatings: bactericidal effect in the lighting and in the darkness. *Ceram. Int.*, 44, 9091–9096. https://doi.org/10.1016/j.ceramint.2018.02.116

[21] Chudinovych, O. V., Myroniuk, D. V., Myroniuk, L. A., Shyrokov, O. V., Danylenko, I. M. (2023). Structure, optical properties and photocatalytic activity of undoped, Nd_2O_3-doped ZnO nanocomposites. *Funct. Mater.*, 30, 1–7. https://doi.org/10.15407/fm30.02.1

[22] Mudavakkat, V. H., Noor-A-Alam, M., Bharathi, K. K., Bharathi, K., Kayani, A., Dissanayake, A., Ramana, Chintalapalle, V. (2011). Structure and AC conductivity of nanocrystalline Yttrium oxide thin films. *Thin Solid Films*, 519, 7947–7950. https://doi.org/10.1016/j.tsf.2011.04.222

[23] Karpyna, V., Myroniuk, L., Myroniuk, D. (2023). Effect of Cobalt Doping on Structural, Optical, and Photocatalytic Properties of ZnO Nanostructures. *Catal. Lett.*, 1–10. https://doi.org/10.1007/s10562-023-04493-x

[24] Sidorenko, S.I., Barabash, R.I. (1997). [*Modern X-ray diffraction analysis of real crystals*], Naukova Dumka, Kiev (in Ukrainian).

[25] Liu, Y., Wei, S., Gao, W. (2015). Ag/ZnO heterostructures and their photocatalytic activity undervisible light: Effect of reducing medium. *J. Hazardous Mater*., 287, 59–68. https://doi.org/10.1016/j.jhazmat.2014.12.045

[26] Ahmad, M., Ahmed, E., Zhang, Y., Khalid, N. R., Xu, J., Ullah, M., Hong, Z. (2013). Preparation of highly efficient Al-doped ZnO photocatalyst by combustion synthesis. *Current Appl. Phys*., 13, 697–704. https:// doi: 10.1016/j.cap.2012.11.008

[27] Zamiri, R., Lemos, A.F., Reblo, A., Ahangar, H. A., Ferreira, J.M.F. (2014). Effects of rare-earth (Er, La and Yb) doping on morphology andstructure properties of ZnO nanostructures prepared by wet chemical method. *Ceram. Int.*, 40, 523–529. http://dx.doi.org/10.1016/j.ceramint.2013.06.034

[28] Damen, T. C., Porto, S.P. S., Tell, B. (1966). Raman effect in zinc oxide. *Phys. Rev*., 142, 570. http://dx.doi.org/10.1103/physrev.142.570

[29] Gruber, Th., Prinz, G.M., Kirchner, C., Kling, R., Reuss, F., Limmer, W., Waag, A. (2004). Influences of biaxial strains on the vibrational and exciton energies in ZnO. *J. Appl. Phys*., 96, 289–293. https://doi.org/10.1063/1.1755433

[30] Schneider, L., Halm, S., Bacher, G., Roy, A., Kruis, F. E. (2006). *Phys Status Solidi C.,* 3, 1014–1017. https://doi.org/10.1002/pssc.200564705

[31] Yang J., Wang R., Yang L., Lang J., Wei M., Gao M., Liu X., Cao J., Li X., Yang N. (2011). Tunable deep-level emission in ZnO nanoparticles via yttrium doping. *J. Alloy Compd.,* 509, 3606–3612. https://doi.org/10.1016/j.jallcom.2010.12.102

[32] Ahmad, M., Ahmed, E., Zhang, Y., Khalid, N. R., Xu, J., Ullah, M., Hong, Z. (2013). Preparation of highly efficient Al-doped ZnO photocatalyst by combustion synthesis. *Current Appl. Phys*., 13, 697–704. https://doi: 10.1016/j.cap.2012.11.008

[33] Kuriakose, S., Satpati, B., Mohapatra, S. (2014) Enhanced photocatalytic activity of Co doped ZnO nanodisks and nanorods prepared by a facile wet chemical method. *Phys Chem Chem Phys*., 16, 12741–12749. https://doi.org/10.1039/C4CP01315H

[34] He, R., Hocking, R. K., Tsuzuki, T. (2012). Co-doped ZnO nanopowders: location of cobalt and reduction in photocatalytic activity, *Mat. Chem. Phys*. 132, 1035–1040. https://doi:10.1016/j.matchemphys.2011.12.061